AGU PUBLICATIONS

Paleoceanography

RESEARCH ARTICLE
10.1002/2014PA002748

Key Points:
- Greenland ice core dust record is strongly influenced by atmospheric transport
- Applying a dust record from the North Pacific as a chronostratigraphic tool
- Reconstructed surface paleoreservoir ages since the end of Heinrich Stadial 2

Supporting Information:
- Table S1
- Text S1

Correspondence to:
S. Serno,
Sascha.Serno@ed.ac.uk

Citation:
Serno, S., G. Winckler, R. F. Anderson, E. Maier, H. Ren, R. Gersonde, and G. H. Haug (2015), Comparing dust flux records from the Subarctic North Pacific and Greenland: Implications for atmospheric transport to Greenland and for the application of dust as a chronostratigraphic tool, *Paleoceanography*, *30*, doi:10.1002/2014PA002748.

Received 3 NOV 2014
Accepted 1 MAY 2015
Accepted article online 5 MAY 2015

©2015. American Geophysical Union. All Rights Reserved.

Comparing dust flux records from the Subarctic North Pacific and Greenland: Implications for atmospheric transport to Greenland and for the application of dust as a chronostratigraphic tool

Sascha Serno[1,2,3], Gisela Winckler[1,4], Robert F. Anderson[1,4], Edith Maier[5], Haojia Ren[1,6], Rainer Gersonde[5], and Gerald H. Haug[7]

[1]Lamont-Doherty Earth Observatory, Columbia University, Palisades, New York, USA, [2]Now at School of GeoSciences, University of Edinburgh, Edinburgh, UK, [3]DFG-Leibniz Center for Surface Process and Climate Studies, Institute of Earth and Environmental Science, University of Potsdam, Potsdam-Golm, Germany, [4]Department of Earth and Environmental Sciences, Columbia University, New York, New York, USA, [5]Alfred Wegener Institute Helmholtz Centre for Polar and Marine Research, Bremerhaven, Germany, [6]Department of Geosciences, National Taiwan University, Taipei, Taiwan, [7]Geological Institute, ETH Zürich, Zürich, Switzerland

Abstract We present a new record of eolian dust flux to the western Subarctic North Pacific (SNP) covering the past 27,000 years based on a core from the Detroit Seamount. Comparing the SNP dust record to the North Greenland Ice Core Project (NGRIP) ice core record shows significant differences in the amplitude of dust changes to the two regions during the last deglaciation, while the timing of abrupt changes is synchronous. If dust deposition in the SNP faithfully records its mobilization in East Asian source regions, then the difference in the relative amplitude must reflect climate-related changes in atmospheric dust transport to Greenland. Based on the synchronicity in the timing of dust changes in the SNP and Greenland, we tie abrupt deglacial transitions in the ^{230}Th-normalized ^{4}He flux record to corresponding transitions in the well-dated NGRIP dust flux record to provide a new chronostratigraphic technique for marine sediments from the SNP. Results from this technique are complemented by radiocarbon dating, which allows us to independently constrain radiocarbon paleoreservoir ages. We find paleoreservoir ages of 745 ± 140 years at 11,653 year B.P., 680 ± 228 years at 14,630 year B.P., and 790 ± 498 years at 23,290 year B.P. Our reconstructed paleoreservoir ages are consistent with modern surface water reservoir ages in the western SNP. Good temporal synchronicity between eolian dust records from the Subantarctic Atlantic and equatorial Pacific and the ice core record from Antarctica supports the reliability of the proposed dust tuning method to be used more widely in other global ocean regions.

1. Introduction

Eolian dust is a major driver in the global climate system through its influence on scattering and adsorption of solar radiation [*Tegen and Fung*, 1994; *Harrison et al.*, 2001], cloud and precipitation properties [*Levin et al.*, 1996; *Kaufman et al.*, 2002], and the oceanic biogeochemical cycles of carbon and nutrients as a result of delivering micronutrients like iron [*Martin*, 1990; *Jickells et al.*, 2005]. Paleorecords of eolian dust can be used to reconstruct climatic conditions in the source regions and large-scale atmospheric transport patterns [e.g., *Fischer et al.*, 2007].

Dust storm activity in the extensive arid regions in China and Mongolia, the Taklimakan desert in northwest China, and the deserts of Inner Mongolia (Tengger, Badain Jaran, and Mu Us), is highest in spring months as a result of the interaction of strong temperature gradients and frequent cyclogenesis events producing cold air surges emerging from Siberia [*Sun et al.*, 2001; *Roe*, 2009]. The interplay of these surges with the orography of the source regions produces strong wind gusts, resulting in enhanced dust storm activity [*Sun et al.*, 2001; *Prospero et al.*, 2002; *Roe*, 2009] and uplift of large amounts of dust into the middle and upper troposphere, the zone of the strong westerly wind jetstream [e.g., *Sun et al.*, 2001]. Lithogenic sediment provenance data [*Pettke et al.*, 2000; *Nagashima et al.*, 2011; *Serno et al.*, 2014] and satellite observations from the Subarctic North Pacific (SNP) [*Husar et al.*, 2001; *Uno et al.*, 2011] provide strong evidence that

Table 1. List of Published Deglacial Surface Water Paleoreservoir Ages From the Western Subarctic North Pacific

Sediment Core Name	Water Depth (m)	Reference	Paleoreservoir Age (year)	Age Range (year B.P.)	Reservoir Age Method
RAMA 44PC	2,980	*Keigwin et al.* [1992]	700	~16,450–6,000	No information
GGC-37	3,300	*Lam et al.* [2013]	770 ± 250	23,037–3,461	No information
CH 84-14	978	*Duplessy et al.* [1989]	960	~18,000–10,000	No information
MD01-2416	2,317	*Sarnthein et al.* [2013]	570 ± 140	13,940–13,640	No information
MD01-2416	2,317	*Sarnthein et al.* [2013]	720 ± 285	14,920–14,050	^{14}C plateau tuning
MD01-2416	2,317	*Sarnthein et al.* [2013]	430 ± 250	16,050–15,250	^{14}C plateau tuning
MD01-2416	2,317	*Sarnthein et al.* [2013]	1,140 ± 195	16,400–16,050	^{14}C plateau tuning
MD01-2416	2,317	*Sarnthein et al.* [2013]	1,480 ± 135	17,580–16,900	^{14}C plateau tuning
MD01-2416	2,317	*Sarnthein et al.* [2013]	1,710 ± 440	18,980–18,000	^{14}C plateau tuning

these dust sources contribute the majority of eolian dust to the SNP sediments. Radiogenic isotope and mineralogical studies of mineral dust deposited in Greenland during the Holocene and last glacial period showed that the Greenland dust originates from the same East Asian dust sources that contribute the majority of dust to the SNP [*Biscaye et al.*, 1997; *Svensson et al.*, 2000; *Bory et al.*, 2002, 2003].

The geochemical evidence for a common dust source in the SNP and Greenland, combined with previous findings of a close atmospheric coupling between the two regions during the last deglaciation [e.g., *Ruth et al.*, 2007; *Max et al.*, 2012; *Kuehn et al.*, 2014; *Praetorius and Mix*, 2014], the transition from the Last Glacial Maximum (LGM; ~23,000–18,000 year B.P.; B.P. = before present = A.D. 1950) into the Holocene (since 11,653 year B.P.), and the availability of a well-dated high-resolution dust record from the North Greenland Ice Core Project (NGRIP) ice core in Greenland for the last ~100 kyr [*Ruth et al.*, 2007], provides the opportunity to study the dominant controlling factor for changes in dust deposition in the two regions.

Precise age determination in marine sediment cores is essential for the interpretation of paleoceanographic changes, especially during times of short-term climatic events with sharp transitions like the last deglaciation. The common chronostratigraphic procedures for this time period, including planktic foraminiferal radiocarbon dating and planktic foraminiferal oxygen isotope tuning, bear a number of shortcomings. Potential shortcomings of the planktic foraminiferal radiocarbon dating technique include (1) the possibility that in specific marine environments, not enough foraminifera are available to perform radiocarbon analyses, (2) reworking of sediment material, and (3) uncertainties due to poorly constrained changes in radiocarbon paleoreservoir ages.

All of these factors significantly affect age determination in marine sediment cores from the SNP [e.g., *Sarnthein et al.*, 2004; *Max et al.*, 2012], where bottom waters are corrosive to calcium carbonate [*Haug et al.*, 1995, 2005]. Although most deep SNP sediments lack significant amounts of calcium carbonate, cores have been recovered from a number of rises and seamounts where sufficient calcium carbonate is available for traditional radiocarbon dating. However, the deglacial history of radiocarbon paleoreservoir age changes in the western SNP is still not well understood. On the one hand, paleoreservoir ages for the time period since ~16,000 year B.P. from the western North Pacific [*Duplessy et al.*, 1989; *Keigwin et al.*, 1992; *Lam et al.*, 2013; *Sarnthein et al.*, 2013] (Table 1) and from the Bering Sea [*Kuehn et al.*, 2014] are generally consistent with observed modern surface water reservoir ages in the coastal region between Kamchatka and northeast Honshu in the western SNP (418–967 years) [*Yoneda et al.*, 2000, 2002, 2004, 2007; *Kuzmin et al.*, 2001, 2007]. On the other hand, different methods indicate a variable paleoreservoir age history during the early deglaciation prior to 16,000 year B.P., including the early Heinrich Stadial 1 (HS1; ~17,500–14,630 year B.P.) and the LGM (Table 1). While older paleoreservoir ages in the range of 945–2150 years, based on tuning planktic foraminiferal radiocarbon plateaus in marine sediment core MD01-2416 from the Detroit Seamount with corresponding plateaus in the terrestrial plant macrofossil radiocarbon "reference" record from Lake Suigetsu, Japan [*Ramsey et al.*, 2012], have been reconstructed prior to 16,000 year B.P. [*Sarnthein et al.*, 2013], other reconstructions indicate constant reservoir ages for the last ~23,000 years in the western SNP [e.g., *Duplessy et al.*, 1989; *Keigwin et al.*, 1992; *Lam et al.*, 2013] (Table 1). Developing and testing new chronostratigraphic techniques is essential to reduce uncertainties in existing methods and to independently constrain surface water paleoreservoir ages in the western SNP and other regions of the global ocean.

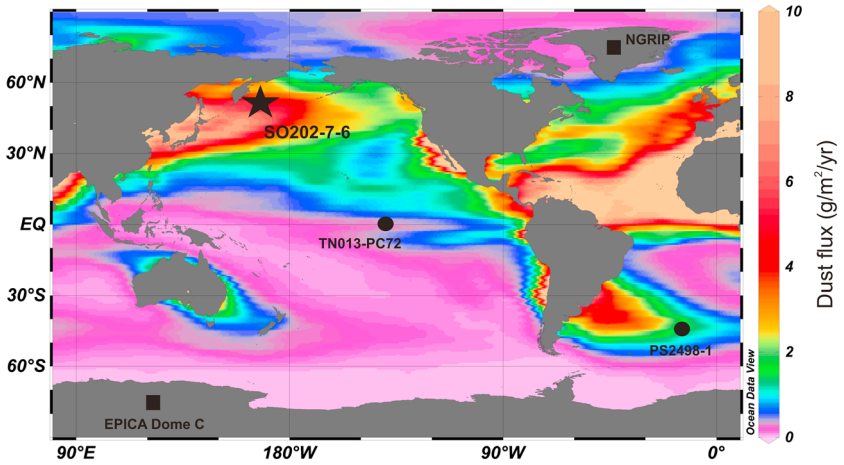

Figure 1. Global map of the modern eolian dust flux [*Mahowald et al.*, 2005]. The location of sediment core SO202-7-6 in the western Subarctic North Pacific (51.3°N, 167.7°E, 2345 m water depth) is indicated by a black star. Locations of other marine sediment cores with dust records referenced in this study are indicated by black points (TN013-PC72 (0.1°N, 139.4°W [*Winckler et al.*, 2008]) and PS2498-1 (44.2°S, 14.5°W [*Anderson et al.*, 2014])). Locations of the two ice cores referenced in this study, NGRIP in Greenland (75.1°N, 42.3°W) and EPICA Dome C in Antarctica (75.1°S, 123.4°E), are indicated by black squares. The map was created using *Ocean Data View 4.6.3.1* [*Schlitzer*, 2014].

Here we present a new high-resolution dust flux record based on ^{4}He from sediment core SO202-7-6 from the Detroit Seamount in the western SNP (51.3°N, 167.7°E, 2345 m water depth; Figure 1) covering the past 27,000 years. The dust flux records from the western SNP and the NGRIP ice core in Greenland [*Ruth et al.*, 2007] show synchronous changes at abrupt climatic transitions during the last deglaciation but substantial differences in their relative amplitudes of deglacial changes, which we relate to climate-related changes in the transport of dust from East Asian sources to Greenland. The synchronicity of the two high-resolution dust records enables us to tie abrupt transitions in the ^{4}He-based dust flux record from sediment core SO202-7-6 to corresponding sharp transitions in the dust record from the NGRIP ice core. The dust tuning is complemented by a high-resolution radiocarbon stratigraphy based on the planktic foraminifera *Neogloboquadrina pachyderma* (sinistral), which allows us to constrain paleoreservoir ages at dust tie points while generating a robust age model for the last 27,000 years.

2. Geochemical Background

2.1. ^{4}He as an Eolian Dust Proxy

Terrestrial ^{4}He (^{4}He$_{terr}$) has been successfully used as an eolian dust proxy in marine sediments [*Patterson et al.*, 1999; *Mukhopadhyay et al.*, 2001; *Winckler et al.*, 2005, 2008; *Marcantonio et al.*, 2009; *Serno et al.*, 2014], Antarctic ice [*Winckler and Fischer*, 2006], and corals [*Mukhopadhyay and Kreycik*, 2008; *Bhattacharya*, 2012]. ^{4}He in continental crust material is produced by α-decay of U/Th-series elements. In source rocks, U and Th are concentrated in accessory mineral phases like zircon or uraninite, which have sufficient helium retentivity to retain radiogenic ^{4}He during weathering [e.g., *Mamyrin and Tolstikhin*, 1984; *Martel et al.*, 1990]. When grains weather to typical grain sizes of long-range transported eolian dust (~2–5 μm) [*Tsoar and Pye*, 1987; *Rea and Hovan*, 1995; *Serno et al.*, 2014], they do not accumulate more ^{4}He from α-decay since the recoil length of α-particles is ~10–30 μm [*Farley*, 1995; *Ballentine and Burnard*, 2002]. Volcanic source rocks have ^{4}He concentrations around 2 to 3 orders of magnitude lower than concentrations of typical continental crust material [*Mamyrin and Tolstikhin*, 1984; *Patterson et al.*, 1999; *Kurz et al.*, 2004; *McGee*, 2009].

The contrast between relatively high ^{4}He concentrations in eolian dust material and negligible concentrations in volcanic input makes ^{4}He a particularly useful proxy for eolian dust input in sediments from the SNP because this region is characterized by large lithogenic input other than eolian dust, including volcanic ash, hemipelagic material, riverine input, or ice-rafted debris (IRD) [e.g., *Olivarez et al.*, 1991; *Bailey*, 1993; *Jones et al.*, 1994, 2000; *McKelvey et al.*, 1995; *Weber et al.*, 1996; *Shigemitsu et al.*, 2007;

Serno et al., 2014]. Because of the geological setting of the surrounding land in the SNP, noneolian contributions to the SNP, like hemipelagic material, riverine input, or IRD, have a geochemical signature similar to fine-grained volcanic ash [e.g., *Jones et al.*, 1994; *McKelvey et al.*, 1995; *Shigemitsu et al.*, 2007] and are virtually ^{4}He-free. Additional confirmation for this approach has been recently provided by a spatial reconstruction of modern eolian dust input with independent geochemical fingerprinting based on rare earth elements and ^{232}Th [*Serno et al.*, 2014]. Therefore, we conclude that ^{4}He provides an estimate of eolian dust that is insensitive to volcanic contributions to the sediments.

Helium isotopes in marine sediments are a binary mixture of terrestrial material and extraterrestrial interplanetary dust particles (IDPs) [e.g., *Patterson et al.*, 1999; *Winckler et al.*, 2005]. Helium is not associated with biogenic or authigenic phases [e.g., *Farley*, 1995; *Patterson et al.*, 1999]. The concentration of sedimentary $^4\mathrm{He}_{\mathrm{terr}}$ can be calculated using a two-component mixing model and the measured ^{4}He concentration ($^4\mathrm{He}_{\mathrm{meas}}$) and helium isotope ratio [$(^3\mathrm{He}/^4\mathrm{He})_{\mathrm{meas}}$] in the sample [*Patterson et al.*, 1999]:

$$^4\mathrm{He}_{\mathrm{terr}} = {}^4\mathrm{He}_{\mathrm{meas}} \times \left\{ \left[\left(^3\mathrm{He}/^4\mathrm{He}\right)_{\mathrm{meas}} - \left(^3\mathrm{He}/^4\mathrm{He}\right)_{\mathrm{IDP}} \right] / \left[\left(^3\mathrm{He}/^4\mathrm{He}\right)_{\mathrm{terr}} - \left(^3\mathrm{He}/^4\mathrm{He}\right)_{\mathrm{IDP}} \right] \right\} \quad (1)$$

with $(^3\mathrm{He}/^4\mathrm{He})_{\mathrm{IDP}}$ = helium isotope ratio of IDPs = 2.4×10^{-4} [*Nier and Schlutter*, 1990, 1992] and $(^3\mathrm{He}/^4\mathrm{He})_{\mathrm{terr}}$ = helium isotope ratio of terrestrial material = 3×10^{-8} [*Mamyrin and Tolstikhin*, 1984; *Farley*, 2001].

2.2. ^{230}Th Normalization

Excess ^{230}Th in the sediments ($\mathrm{xs}^{230}\mathrm{Th}_0$) has been established as a constant-flux proxy [e.g., *Bacon*, 1984; *Henderson et al.*, 1999; *Francois et al.*, 2004; *Anderson et al.*, 2006]. Production of ^{230}Th occurs in the water column by α-decay of ^{234}U. Due to the short residence time of ^{230}Th in the water column as a result of efficient particle scavenging (<40 years) [e.g., *Bacon and Anderson*, 1982; *Anderson et al.*, 1983; *Henderson et al.*, 1999; *Francois et al.*, 2004], its scavenged flux to the seafloor is approximately equal to its production rate ($\beta_{230} = 2.67 \times 10^{-5}$ dpm/cm^3/kyr) in the overlying water column [*Francois et al.*, 2004]. Mass accumulation rates (MARs) estimated using this approach offer advantages over conventional stratigraphic MARs in that the ^{230}Th-normalized fluxes are insensitive to lateral sediment redistribution, are only slightly sensitive to age model uncertainties, are determined for every sample, and do not rely on the determination of dry bulk density [e.g., *Henderson et al.*, 1999; *Francois et al.*, 2004; *Anderson et al.*, 2006]. The ^{230}Th-normalized MAR for a constituent *i*, MAR_i, with a concentration c_i in the sediment deposited at a specific water depth *z* was calculated following the method described in *Francois et al.* [2004]:

$$\mathrm{MAR}_i = (c_i \times \beta_{230} \times z) / \mathrm{xs}^{230}\mathrm{Th}_0 \quad (2)$$

$\mathrm{xs}^{230}\mathrm{Th}_0$ (in dpm/g) is corrected for radioactive decay since its time of deposition, the fraction supported by uranium within lithogenic material (mean detrital $^{238}\mathrm{U}/^{232}\mathrm{Th} = 0.5 \pm 0.1$) [*Taguchi and Narita*, 1995] and the fraction of the in situ ^{230}Th produced by decay of authigenic ^{238}U [*Francois et al.*, 2004; *Anderson et al.*, 2006].

3. Material and Methods

Samples have been derived from box sediment core SO202-7-6 from the Detroit Seamount in the western SNP (Figure 1), recovered during the SO202-INOPEX cruise in 2009 [*Gersonde*, 2012]. Sediment core SO202-7-6 was sampled every 2 cm between 100.5 and 24.5 cm core depth, and every 4 cm between 24.5 and 4.5 and between 128.5 and 100.5 cm core depth, respectively, for helium and U/Th isotope analyses. All data presented in this manuscript are reported in Table S1 in the supporting information.

3.1. Helium Isotopes

Between 70 and 230 mg of freeze-dried hand-crushed bulk sediment was wrapped in aluminum foil cups and loaded into the vacuum furnace of the gas inlet system and analyzed for helium isotopes on a MAP 215–50 mass spectrometer at the Lamont-Doherty Earth Observatory (LDEO) following the procedure described in *Winckler et al.* [2005]. Calibration was performed every 4–5 samples using a known volume of a standard gas with a helium isotope ratio of 16.45 R_A (with $R_A = {}^3\mathrm{He}/^4\mathrm{He}$ in air = 1.384×10^{-6}). Standard reproducibility was ~0.5% (1σ) for ^{4}He and ~1.5% (1σ) for $^3\mathrm{He}/^4$He. Procedural blanks yielded ~0.1 ncc STP of ^{4}He (ncc STP = nano cubic centimeter at standard temperature and pressure) with atmospheric isotopic composition and represented blank corrections of <1% ^{4}He for the samples. For 21 samples, we analyzed

2–4 replicates, with an average reproducibility of 8.7% (1σ) for ^{4}He. The contribution of $^4He_{terr}$ to total ^{4}He is >98% for all samples.

3.2. U/Th Isotope Analyses

For U/Th isotopes, ~200 mg of freeze-dried and hand-crushed bulk sediment was weighed into 50 mL Teflon beakers and spiked with ^{229}Th and ^{236}U prior to a complete acid digestion and anion exchange chromatography following the method of *Fleisher and Anderson* [2003]. Samples were analyzed by isotope dilution using a high-resolution Element XR ICP-MS at LDEO. ^{238}U concentrations were derived using the measured ^{235}U/^{236}U and a ^{238}U/^{235}U ratio of 137.88 for the SRM129 standard [*Steiger and Jäger*, 1977], measured with every batch of 21 samples and one procedural blank. Blank corrections were <1.5% and average analytical reproducibility <2.2% (1σ) for ^{230}Th, ^{232}Th, and ^{238}U. Long-term reproducibility, based on multiple analyses of a surface sediment sample from the INOPEX cruise, is 2.2% (1σ) for ^{230}Th, 2.4% (1σ) for ^{232}Th, and 4.2% (1σ) for ^{238}U. Reproducibility of 2–3 replicates from 15 of the SO202-7-6 samples is 2.5% (1σ) for ^{230}Th, 2.6% (1σ) for ^{232}Th, and 2.9% (1σ) for ^{238}U.

3.3. Planktic Foraminiferal Radiocarbon Analyses

The planktic foraminifera *Neogloboquadrina pachyderma* (sinistral), a subsurface-dwelling species living at ~50–200 m water depth in the North Pacific [*Kuroyanagi et al.*, 2002], was picked from the >150 μm fraction in 40 samples between midcore depths of 130.5 and 4.5 cm for accelerator mass spectrometry (AMS) radiocarbon analyses. Each sample has a 1 cm core depth resolution. AMS radiocarbon analyses were performed on ~5–10 mg of planktic foraminifera at the National Ocean Science Accelerator Mass Spectrometry (NOSAMS) facility at the Woods Hole Oceanographic Institution in Woods Hole, Massachusetts, USA, and at the ETH accelerator facility in Zürich, Switzerland. Radiocarbon ages are reported according to the convention outlined by *Stuiver and Pollach* [1977] and *Stuiver* [1980]. For two core depths (50.5 and 56.5 cm), duplicate measurements were performed, with radiocarbon ages of 11,850 ± 50 years and 12,286 ± 47 years for 50.5 cm and 12,812 ± 50 years and 12,850 ± 50 years for 56.5 cm core depth. The reason for the offset between the measured radiocarbon ages at 50.5 cm is uncertain. For the following conversion of radiocarbon to calendar ages, we used the average of the duplicate measurements, with the uncertainty representing the deviation of the duplicates (12,068 ± 218 years for 50.5 cm and 12,831 ± 19 years for 56.5 cm). Conversion of radiocarbon to calendar ages was performed using the downloadable version of Calib 7.0.4 (http://calib.qub.ac.uk/calib/calib.html) [*Stuiver and Reimer*, 1993] with the Marine13 calibration curve [*Reimer et al.*, 2013] and a laboratory error of 0. The Marine13 calibration incorporates a global ocean reservoir correction of ~400 years. Using the Marine13 calibration curve in Calib 7.0.4, an estimate of ΔR, the difference in reservoir age of the local region of interest and the model ocean [*Reimer et al.*, 2013], has to be provided. All reservoir ages reported here are total reservoir ages, including the global reservoir age correction of 400 years and ΔR. We selected the reported 2σ calibrated calendar age range of the probability distribution [*Telford et al.*, 2004]. To generate point estimates, we used the reported median of the probability distribution, with the deviation of the upper and lower limits of the reported 2σ range from the median as an upper and lower error estimate. All calendar ages are reported in year B.P.

4. Results and Discussion

4.1. Terrestrial ^{4}He Concentrations and Fluxes

The $^4He_{terr}$ concentration record shows large changes over the sampled interval. Concentrations are ~700–900 ncc STP g^{-1} from 128.5 to 66.5 cm, with a nearly monotonic decrease from bottom to top (Figure 2a). Between 66.5 and 60.5 cm core depth, $^4He_{terr}$ concentrations drop rapidly to ~350 ncc STP g^{-1} and stay low until 52.5 cm core depth, when concentrations increase from ~450 to 700 ncc STP g^{-1}. $^4He_{terr}$ remains high until 40.5 cm core depth and then drops to ~350 ncc STP g^{-1} within a narrow depth range of 6 cm, followed by a slight decrease to constant values of ~200 ncc STP g^{-1} between 26.5 cm and the core top.

The ^{230}Th-normalized $^4He_{terr}$ flux record shows relatively constant fluxes of ~15,000 ncc STP/m^2/yr between 104.5 and 66.5 cm core depth and elevated fluxes of ~17,000–22,000 ncc STP/m^2/yr between 128.5 and 104.5 cm, with a pronounced peak at 112.5 cm core depth and a sharp decrease between 112.5 and 104.5 cm core depth (Figure 2b). Between 66.5 and 60.5 cm, $^4He_{terr}$ fluxes decrease, but less pronounced than $^4He_{terr}$ concentrations, and then constantly increase to ~18,000 ncc STP/m^2/yr at 40.5 cm core depth. $^4He_{terr}$ fluxes

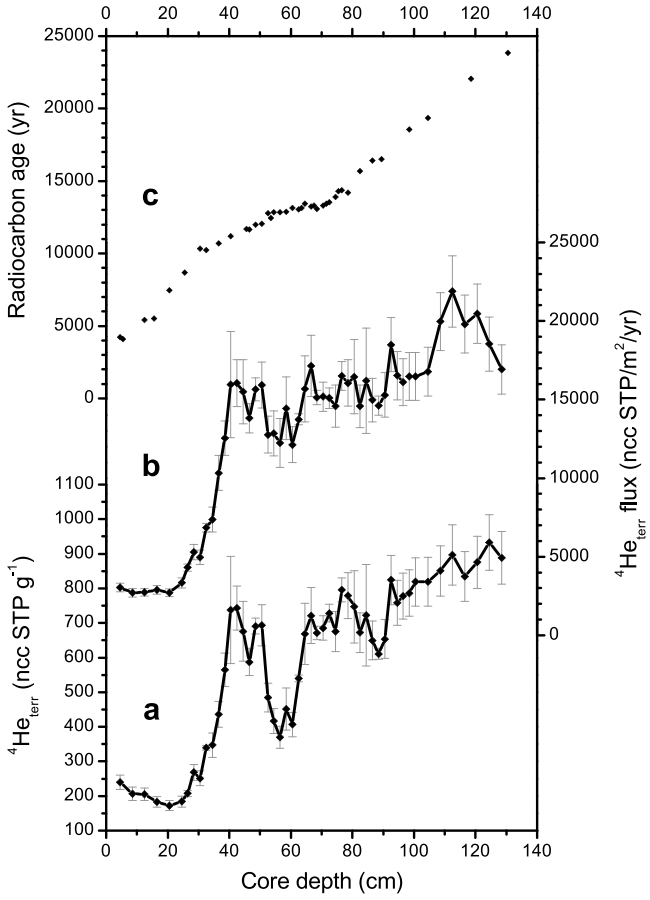

Figure 2. (a) $^4He_{terr}$ concentrations, (b) $^4He_{terr}$ fluxes, and (c) uncorrected planktic foraminiferal radiocarbon dates from marine sediment core SO202-7-6 in the western SNP plotted over core depth. The error bars represent the total propagated uncertainty from all sources. Point-to-point precision in evaluating relative changes over time is estimated to be much better, as indicated by smooth transitions across many of the features in the $^4He_{terr}$ records.

rapidly drop to ~7000 ncc STP/m^2/yr between 40.5 and 34.5 cm, and then tail off to constant low fluxes of ~3000 ncc STP/m^2/yr between 26.5 cm and the core top.

4.2. Comparison of Timing and Amplitude of Deglacial Dust Flux Changes in the Western Subarctic North Pacific and Greenland

We reconstructed dust fluxes for the NGRIP ice core using the published dust concentration data [*Ruth et al.*, 2007], reconstructed ice accumulation rates for the NGRIP ice core, and the density of ice (917 kg/m^3). Throughout the manuscript, we use the most recent published time scale for the NGRIP ice core, the GICC05modelext time scale [*Andersen et al.*, 2006; *Rasmussen et al.*, 2006; *Vinther et al.*, 2006; *Svensson et al.*, 2008; *Wolff et al.*, 2010]. Ice accumulation rates were reconstructed by correcting λ (the annual ice layer thickness) for ice layer thinning as a result of plastic deformation (Anders Svensson, University of Copenhagen, personal communication, 2014), using the results of strain from the thinning function for the NGRIP ice core (after *Johnsen et al.* [2001]). The reconstructed NGRIP dust flux record shows a remarkable correspondence to the proxy record of regional temperature based on oxygen isotopes, with sudden transitions between short-term deglacial climatic events occurring within a few years to decades (Figures 3a and 3b) [*Ruth et al.*, 2007; *Steffensen et al.*, 2008]. Higher eolian dust flux during the cold stadials (LGM, HS1, and the Younger Dryas stadial (YD) between 12,800 and 11,653 year B.P.) and lower eolian dust fluxes during the warm Bølling/Allerød (B/A; 14,630–12,800 year B.P.) and Holocene characterize the deglacial period in these records (Figures 3a and 3b). Dust supply is high during Heinrich Stadial 2 (HS2; 24,210–23,290 year B.P.).

The eolian dust supply to a deposition site far away from the source region is influenced by a variety of factors, including the dust source strength, as a result of changes in the source area aridity, rock weathering, soil surface conditions and vegetation cover, and the dust transport from source to deposition site, which is influenced by changes in the dust transport path, wind intensity, and local precipitation. Since both the SNP and Greenland share the same primary dust source in East Asia, comparison of the dust deposition records from both regions should give valuable information about changes in the dust transport or source strength.

For a direct comparison of the temporal variability in the ^{230}Th-normalized $^4He_{terr}$ flux and $^4He_{terr}$ concentration records from SO202-7-6, as an indicator of eolian dust input to the western SNP, and the NGRIP dust flux record, we first constructed a preliminary age model for SO202-7-6. This preliminary age model is based on the planktic foraminiferal radiocarbon dates from SO202-7-6. We used a constant total paleoreservoir age of 700 years [*Keigwin et al.*, 1992] to convert the radiocarbon to calendar ages in SO202-7-6. For time periods of constant radiocarbon ages (Table 2 and Figure 2c), we did not estimate a calibrated calendar age

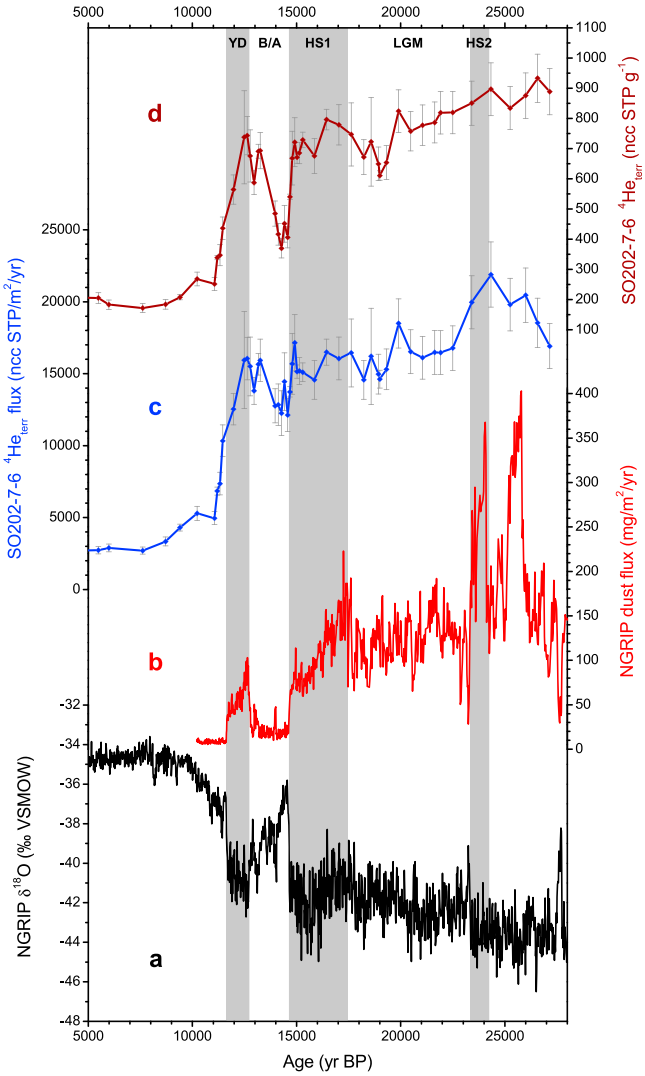

Figure 3. Comparison of (a) the oxygen isotope record from the NGRIP ice core in Greenland [*Andersen et al.*, 2006; *Rasmussen et al.*, 2006; *Vinther et al.*, 2006] and (b) the NGRIP dust flux record (dust concentration data published in *Ruth et al.* [2007]), plotted on the GICC05modelext time scale, with (c) the $^4He_{terr}$ flux and (d) $^4He_{terr}$ concentration records from SO202-7-6. The three grey bars indicate Heinrich Stadial 2 (HS2; 24,210–23,290 year B.P.), Heinrich Stadial 1 (HS1; 17,500–14,630 year B.P.), and the Younger Dryas stadial (YD; 12,800–11,653 year B.P.). Time periods in between the grey bars are the Last Glacial Maximum (LGM; ~23,000–18,000 year B.P.) and the Bølling/Allerød (B/A; 14,630–12,800 year B.P.). The data from SO202-7-6 are plotted on a preliminary age model based on the planktic foraminiferal radiocarbon dates and a constant total paleoreservoir age of 700 year [*Keigwin et al.*, 1992]. See section 4.2 for further information.

from the available radiocarbon samples. Ages for these intervals have been assigned through linear interpolation between age tie points at the end and beginning of these intervals. For all other core depths in SO202-7-6, calendar ages were assigned by assuming constant sediment accumulation rates between the nearest two radiocarbon samples. Later, we further refine the age model of SO202-7-6.

Comparing the SO202-7-6 dust deposition record on the preliminary age scale with the NGRIP dust flux record indicates that the dust flux changes observed in Greenland during the last 27,000 years are well defined in SO202-7-6 (Figure 3). This is particularly true for the sudden transition from high dust in HS1 into the less dusty B/A, followed by the dustier YD and a sudden transition into the early Holocene with lower dust fluxes. However, although the general patterns in the eolian dust flux records from Greenland and the western SNP show a good temporal correspondence, we observe significant differences in the magnitude of dust flux changes between the two regions (Figure 4). Dust fluxes to Greenland are amplified by a factor of ~13–20 during the LGM and HS1 compared to the Holocene, thereby indicating a much greater relative change in eolian dust flux compared to the corresponding relative dust flux change in the western SNP with an amplification by a factor of ~5. Furthermore, the dust flux in Greenland nearly drops to Holocene levels during the B/A, in contrast to the much smaller decrease in the western SNP.

If the SO202-7-6 record faithfully tracks nearby eolian dust sources in East Asia, then the much larger amplitude of dust flux variability in Greenland must be attributed largely to changes in atmospheric dust transport rather than changes in East Asian dust source strength. The atmospheric dust transport efficiency can be influenced by the wind strength, by the atmospheric transport paths from East Asia to Greenland, and by the rate of aerosol rainout during the transport from the source to deposition site [e.g., *Fischer et al.*, 2007].

During stadials, an increased meridional temperature gradient as a result of increased sea ice coverage, more extensive ice sheets, and/or diminished overturning circulation in the North Atlantic is thought to result in a more vigorous atmospheric circulation in the Northern Hemisphere, including stronger northern westerlies

Table 2. Core Depth Intervals With Constant Radiocarbon Ages[a]

Depth Interval (cm)	Age Control Point at the Beginning of Interval (cm)	Age Control Point at the End of Interval (cm)	Radiocarbon Age Samples Within Interval[b] (cm)
12–4.5	12.5	4.5	5.5
36–30.5	36.5	30.5	32.5
48–45.5	48.5	45.5	46.5
60–52.5	60.5	52.5	53.5, 54.5, 56.5, 58.5
71–60.5[c]	71.5	60.5	62.5, 63.5, 64.5, 66.5, 67.5, 68.5, 70.5
82–76.5	82	76.5	78.5

[a]Ages within these intervals have been linearly interpolated between the age model tie points at the beginning and end of the intervals.
[b]Radiocarbon ages from these samples were not used for construction of final age chronology of SO202-7-6.
[c]Ages within this core interval linearly interpolated using the radiocarbon dates at 71.5 and 60.5 cm core depth and the dust tie point at 63.5 cm core depth.

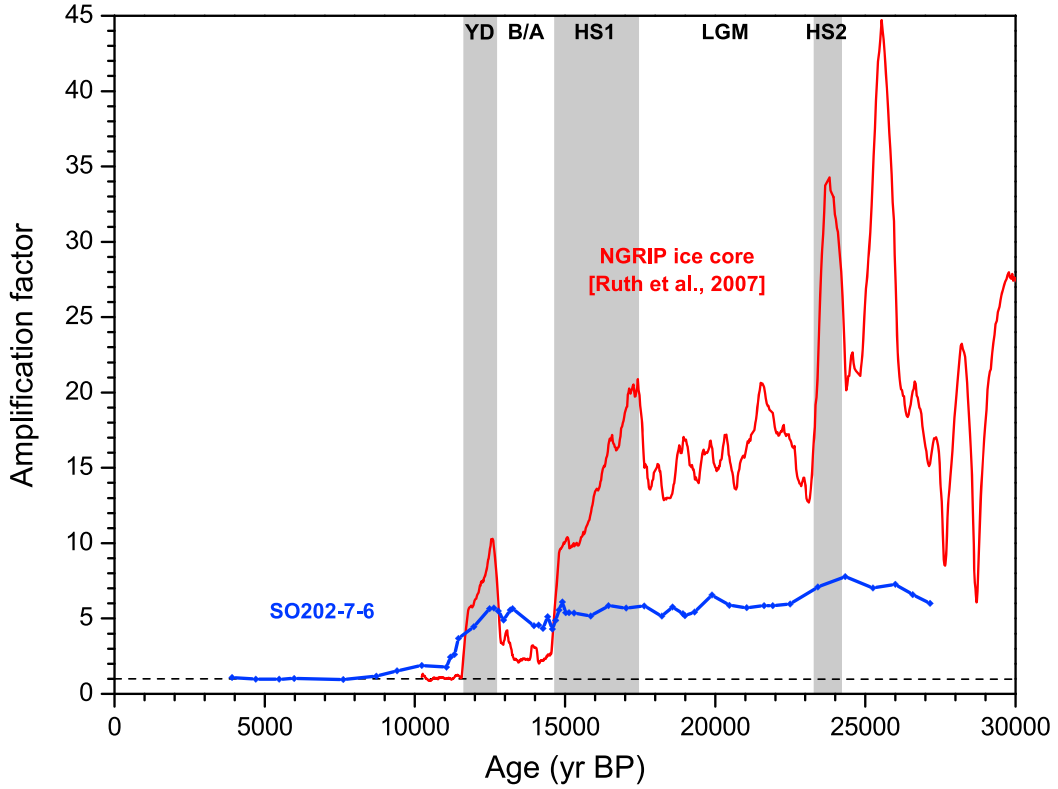

Figure 4. Graphic illustration of the amplification factor for eolian dust fluxes recorded in the western SNP and Greenland over the last deglaciation, in comparison to Holocene fluxes. The $^4He_{terr}$ flux record from SO202-7-6 (blue line and squares) (this study; plotted on preliminary age model based on the planktic foraminiferal radiocarbon dates and a constant total reservoir age of 700 year) is compared to the NGRIP dust flux record (red line), with the NGRIP record plotted on the GICC05modelext time scale and smoothed by using weighted averages for 15 data points per window. The dashed horizontal line indicates the reference level for the normalization. We normalized to the median of flux values from 9000 to 3000 year B.P. for the $^4He_{terr}$ flux record (constant Holocene fluxes) and to the median of fluxes from 11,000 to 10,000 year B.P. for the NGRIP dust flux record, respectively. We normalize the NGRIP dust fluxes to the median from 11,000 to 10,000 year B.P. because the NGRIP dust concentration record from *Ruth et al.* [2007] ends at ~10,000 year B.P. This is justified by the GISP2 Ca^{2+} record, with Ca^{2+} in ice serving as an eolian dust indicator. The GISP2 Ca^{2+} record shows little change in dust deposition in Greenland during the past 11,000 years [*Mayewski et al.*, 1997]. YD: Younger Dryas stadial, B/A: Bølling/Allerød interstadial, HS1 and HS2: Heinrich Stadials 1 and 2, LGM: Last Glacial Maximum.

[e.g., *Svensson et al.*, 2000; *Tegen and Rind*, 2000; *Fischer et al.*, 2007; *Ruth et al.*, 2007]. This vigorous atmospheric circulation can explain the strong coupling between regional climate signals in Greenland and East Asia on time scales of a few years to decades [e.g., *Porter and An*, 1995; *Ruth et al.*, 2007; *Yancheva et al.*, 2007; *Nagashima et al.*, 2011; *Sun et al.*, 2012]. Besides stronger northern westerlies and higher cyclonic activity, atmospheric and coupled atmosphere-ocean circulation models provide evidence for modified atmospheric transport paths from East Asia to Greenland as a result of a more extensive Laurentide Ice Sheet during stadials. The extensive Laurentide Ice Sheet represents a topographic barrier to the westerly jet stream, resulting in a split of the jet into a northern branch (over Alaska and the Canadian Arctic) and a southern branch south of the ice sheet (present central and southern United States) [e.g., *Kutzbach and Wright*, 1985; *Manabe and Broccoli*, 1985; *Bush and Philander*, 1999; *Bromwich et al.*, 2004]. The northern branch of this split jet would represent a shortened transport pathway from East Asian deserts to Greenland [e.g., *Fischer et al.*, 2007; *Ruth et al.*, 2003].

The importance of the variability of the Laurentide Ice Sheet for wind shifts has also been pointed out by *Wunsch* [2006]. He suggested that Dansgaard/Oeschger events during the last glacial period were a consequence of interactions of the wind field with the continental ice sheets, driving rapid changes in ocean circulation, and pronounced temperature and precipitation changes. Further, a Northern Hemisphere-wide decrease in precipitation has been reconstructed for stadials in modeling studies [e.g., *Tegen and Rind*, 2000], possibly resulting in decreased wet deposition of dust on its way from its East Asian source to the deposition site in Greenland [*Tegen and Rind*, 2000; *Fischer et al.*, 2007]. All these factors (more vigorous atmospheric circulation, split of jet stream, and decreased precipitation) can play a role in explaining the higher transport efficiency of eolian dust from East Asia to Greenland during stadials, leading to observed differences in relative dust flux changes between Greenland and the western SNP.

While relative dust flux changes between Greenland and the western SNP show differences, the apparent synchronicity in the patterns of sudden transitions in the records suggests that the timing of abrupt dust flux changes during the last deglaciation was synchronous in both regions. Support for this assumption comes from geochemical evidence for a common dust source in the western SNP and Greenland [*Biscaye et al.*, 1997; *Svensson et al.*, 2000; *Bory et al.*, 2002, 2003] and previous findings of a close atmospheric coupling between the two regions during the last deglaciation and Holocene [e.g., *Ruth et al.*, 2007; *Max et al.*, 2012; *Kuehn et al.*, 2014; *Praetorius and Mix*, 2014]. Further, different components of Earth's climate system are likely to change concurrently during periods of abrupt climate change [e.g., *Alley et al.*, 2003], a feature that has been extensively used in paleoceanographic studies to line up transitions in records of the same parameter between different regions [e.g., *Pisias et al.*, 1984; *Martinson et al.*, 1987]. Therefore, changes in the atmospheric transport patterns between the two regions, as we argue above, likely lead to relative changes in the amplitude but not necessarily change the pattern of timing. The synchronicity in the timing of sudden dust flux changes in Greenland and the SNP enables the tying of the sudden transitions in the records from SO202-7-6 to corresponding transitions in the well-dated dust flux record from Greenland to reconstruct deglacial paleoreservoir ages in the western SNP and to further refine the age model for SO202-7-6.

4.3. Dust Record Tuning Between Greenland and the Subarctic North Pacific

While transitions in the marine records are not as abrupt as in ice core records due to a lower sampling resolution and bioturbation in marine sediments, we can identify three tie points in the coupled eolian dust records: the midtransitions from the YD into the early Holocene interglacial and from HS1 into the B/A, as well as the midtermination of HS2 (cf. Figures 5a and 5b). The midtransition from the YD into the early Holocene interglacial at 11,653 ± 50 year B.P. at NGRIP [*Rasmussen et al.*, 2006] can be tied to the sudden transition from high to low $^4He_{terr}$ fluxes and concentrations between 40.5 and 34.5 cm core depth, with the midpoint of the transition at 37.5 cm as the tie point (Figure 5 and Table 3). The tailing off in the SO202-7-6 records following the sharp decrease characterizing the YD-early Holocene transition (Figures 5b and 5c) is a common, yet not fully understood, feature in other global paleoceanographic records at this time [e.g., *Keigwin*, 1998; *McManus et al.*, 2004]. We therefore define the transition in SO202-7-6 as the sharp decrease until the tailing off begins at 34.5 cm core depth. The midtransition from the dusty HS1 into the B/A at 14,630 ± 93 year B.P. [*Andersen et al.*, 2006] can be tied to the midpoint of the sudden transition from high to low $^4He_{terr}$ fluxes and concentrations between 66.5 and 60.5 cm core depth (63.5 cm as the tie point;

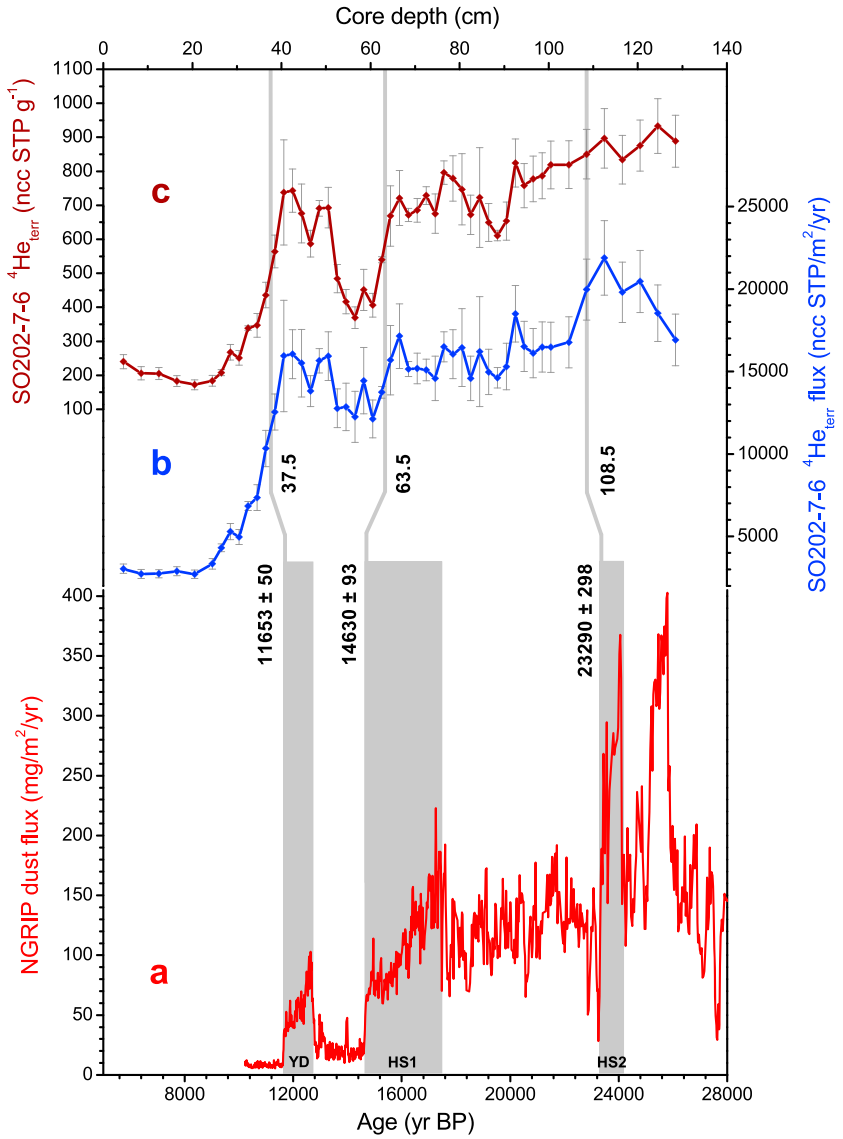

Figure 5. Comparison of (a) the NGRIP dust flux record, plotted on the GICC05modelext time scale, with (b) the $^4He_{terr}$ flux and (c) $^4He_{terr}$ concentration records from SO202-7-6 plotted against core depth. The three grey bars in (a) indicate HS2, HS1, and the YD. The dark grey lines show the match-up of the YD-early Holocene and HS1-B/A midtransitions between the NGRIP dust flux (11,653 ± 50 and 14,630 ± 93 year B.P., respectively) and $^4He_{terr}$ flux and concentration records (37.5 and 63.5 cm core depth, respectively), as well as the match-up of the HS2 midtermination in the NGRIP dust flux record at 23,290 ± 298 year B.P. with the midtransition from high to lower $^4He_{terr}$ fluxes at 108.5 cm core depth in SO202-7-6.

Figure 5 and Table 3). The midtermination of HS2 at 23,290 ± 298 year B.P. in the NGRIP climatic records [*Andersen et al.*, 2006] corresponds to the transition from high to low $^4He_{terr}$ flux between 112.5 and 104.5 cm core depths in SO202-7-6, with the tie point set at 108.5 cm (Figure 5 and Table 3). Consequently, we use each of the dust-derived age control points to refine the age model for SO202-7-6.

4.4. Deglacial Changes of Surface Water Paleoreservoir Ages in the Western Subarctic North Pacific

Incorporating the three dust tie points into the high-resolution planktic foraminiferal radiocarbon stratigraphy allows us to determine radiocarbon paleoreservoir ages at the tie points. For the tie point at 63.5 cm core depth, we used the measured planktic foraminiferal radiocarbon date at this core depth. For the tie points at 37.5 and 108.5 cm core depth, for which we do not have a measured radiocarbon age, we linearly interpolated between the two neighboring planktic foraminiferal radiocarbon dates (Table S1 in

Table 3. List of the Three Dust Tie Points in Sediment Core SO202-7-6, With Core Depth, Radiocarbon Age With Uncertainty, Calendar Age, Paleoreservoir Ages for the Midpoint, 33% of the Distance From the Midpoint to the Beginning and End of the Dust Transitions (See Section 4.4 for More Details), and Resulting Reported Paleoreservoir Ages With Uncertainties

			Paleoreservoir Age (year)			
Core Depth (cm)	Radiocarbon Age (year)	Calendar Age With Uncertainty (year B.P.)	*Midpoint of Dust Transition*	*33% to Beginning of Transition*[a]	*33% to End of Transition*[a]	Reported Paleoreservoir Age With Uncertainty (year)
37.5	10,825 ± 40	11,653 ± 50[b]	745	885	640	745 ± 140
				870	615	
				850	605	
63.5	13,150 ± 45	14,630 ± 93[c]	680	1,010	615	680 ± 228
				980	580	
				955	555	
108.5	20,135 ± 56	23,290 ± 298[c]	790	1,290	780	790 ± 498
				1,045	535	
				805	295	

[a]We present three estimates of total paleoreservoir age for each dust tie point for the radiocarbon age at the depth 33% of the distance from the midpoint to the beginning and end of the dust transitions. The first value is for a reported calendar age minus uncertainty (11,603 year B.P. for 37.5 cm, 14,537 year B.P. for 63.5 cm, and 22,992 year B.P. for 108.5 cm core depth), the second for the reported calendar age (11,653, 14,630 and 23,290 year B.P., respectively), and the third for the reported calendar age plus uncertainty (11,703, 14,723, and 23,588 year B.P., respectively).
[b]Calendar age for midtransition from *Rasmussen et al.* [2006].
[c]Calendar age for midtransition from *Andersen et al.* [2006].

the supporting information). The uncertainty of the interpolated radiocarbon ages reflects the propagated error from the two neighboring radiocarbon dates.

The reported paleoreservoir age for each dust tie point is the reservoir age at which the median of the probability distribution for the radiocarbon date in Calib 7.0.4 matches the reported calendar age of the three tie points (11,653, 14,630 and 23,290 year B.P., respectively; Table 3), using the conversion approach presented in section 3.3. We applied an empirical approach to estimate uncertainties for the paleoreservoir ages. Starting at the depth of the dust tie point, we selected the depths corresponding to 33% of the distance from the dust tie point to the beginning and end of the dust transition (38.5 and 36.5 cm for the YD-early Holocene transition, 64.5 and 62.5 cm for the HS1-B/A transition, and 109.8 and 107.2 cm for the HS2 termination; Figure 6). For those core depths, we estimated the radiocarbon age by linear interpolation between the two neighboring foraminiferal radiocarbon dates. For the two core depths at 33% of the distance from the dust tie point, we reconstructed the paleoreservoir ages at which the median of the probability distribution matches the reported calendar age (11,653, 14,630 and 23,290 year B.P., respectively), the reported calendar age minus calendar age uncertainty (11,603, 14,537 and 22,992 year B.P., respectively), and the reported calendar age plus calendar age uncertainty (11,703, 14,723 and 23,588 year B.P., respectively; Table 3). The reported uncertainty for the paleoreservoir age of the dust tie

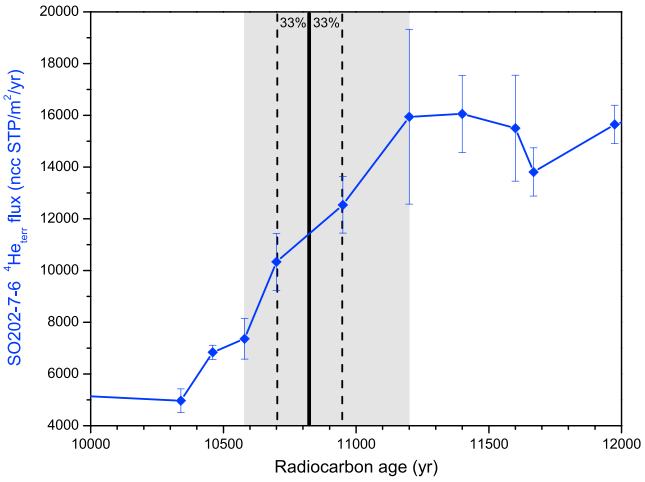

Figure 6. Graphic illustration for the approach to calculate the paleoreservoir age uncertainty for the YD-early Holocene transition. Radiocarbon ages for the core depths of $^4He_{terr}$ flux measurements are linearly interpolated from the dates of analyzed radiocarbon samples in SO202-7-6. The grey bar marks the time period of the YD-early Holocene transition (40.5–34.5 cm core depth), and the solid vertical black line marks the midtransition with a calendar age of 11,653 year B.P. (37.5 cm core depth). The radiocarbon age of the midtransition provides our best estimate of the paleoreservoir age. The two dashed vertical lines are at 33% of the distance from the midpoint of the transition to the start and end of the transition (34.5 and 40.5 cm core depth, respectively). We have performed the same approach for the other two dust tie points, as explained in the text.

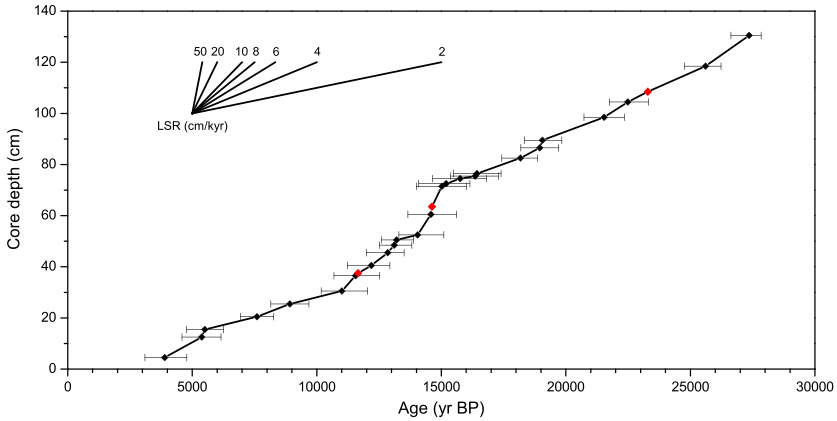

Figure 7. Calibrated calendar ages versus core depth for the dust tie points (red squares) and the planktic foraminiferal radiocarbon samples (black squares) used to construct the final age model of SO202-7-6. LSR—linear sedimentation rates (cm/kyr).

points is estimated as the mean of the maximum deviations between the paleoreservoir age of the midpoint and the three paleoreservoir ages for the core depths at 33% of the distance from the midpoint to the beginning and end of the transition.

As a result of our reservoir age reconstruction, our paleoreservoir ages are 745 ± 140 years for the YD-early Holocene midtransition, 680 ± 228 years for the HS1-B/A midtransition, and 790 ± 498 years for the HS2 midtermination (Table 3). The calculated reservoir ages for the intervals spanning the midtransition of HS2, the transition from HS1 to B/A, and the YD-early Holocene transition fall in a relatively narrow range, within the range of observed modern surface water reservoir ages in the western SNP (418–967 years) [*Yoneda et al.*, 2000, 2002, 2004, 2007; *Kuzmin et al.*, 2001, 2007]. They are also in good correspondence with reconstructed constant paleoreservoir ages since 16,000 year B.P. in the western SNP [*Duplessy et al.*, 1989; *Keigwin et al.*, 1992; *Lam et al.*, 2013; *Sarnthein et al.*, 2013] (Table 1) and with studies assuming a relatively constant paleoreservoir age in the range of modern reservoir ages throughout the entire last deglaciation in the western SNP [e.g., *Ahagon et al.*, 2003; *Ikehara et al.*, 2006; *Max et al.*, 2012] and Bering Sea [*Kuehn et al.*, 2014].

Our results are in contrast to a study from nearby core MD01-2416, with older paleoreservoir ages of 945–2150 years reconstructed before 16,000 year B.P. early in the last deglaciation [*Sarnthein et al.*, 2013] (Table 1). We do not have a paleoreservoir age estimate between the midtermination of HS2 and the HS1-B/A transition and cannot directly evaluate paleoreservoir ages during the LGM and HS1. However, considering the relatively old paleoreservoir ages inferred by *Sarnthein et al.* [2013] for the time period between 18,980 and 16,050 year B.P., in comparison to our reconstructed paleoreservoir ages of 790 ± 498 years at the HS2 termination and 680 ± 228 years at the HS1-B/A transition, one would have to conclude that either there were two major reorganizations in the oceanic carbon system between the end of HS2 and HS1 in the western SNP, leading first to a substantial increase in reservoir age and then to a return to the original value, or that the radiocarbon plateau method overestimates paleoreservoir ages during the LGM and early deglaciation. Future paleoceanographic studies should attempt to evaluate if there were two major reorganizations in the water column stability of the western SNP during the LGM and HS1.

4.5. Construction of the Age Model of SO202-7-6

The dust tie points were combined with the planktic foraminiferal radiocarbon stratigraphy to refine the age model of SO202-7-6 (Figure 7). Since the paleoreservoir ages from the three dust tie points overlap within their estimated uncertainties, we used the mean of the three ages of 738 years and the uncertainty in the average of 326 years to convert the planktic foraminiferal radiocarbon to calendar ages. For time periods of constant radiocarbon ages (Table 2), we did not estimate a calibrated calendar age from the available radiocarbon samples and ages for these intervals have been assigned through linear interpolation

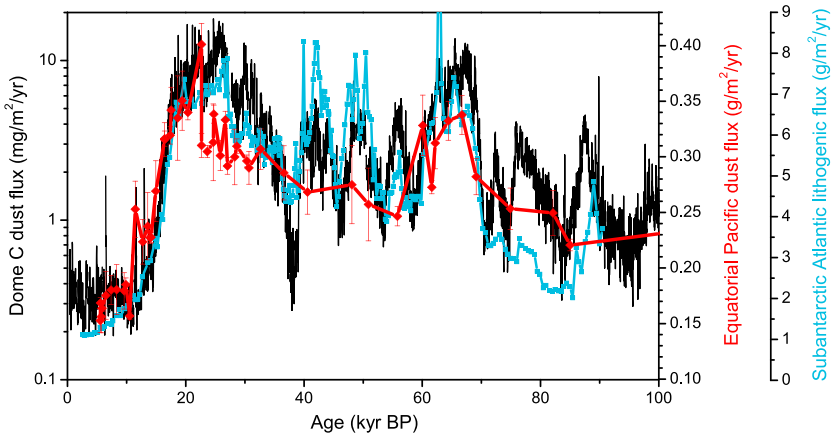

Figure 8. Examples illustrating the potential for global eolian dust records to be used as a chronostratigraphic tool for marine sediment cores. Two marine sediment records of dust flux based on ^{232}Th, one from the equatorial Pacific (red line and diamond symbols; TN013-PC72) [*Winckler et al.*, 2008] and the other from the Subantarctic Atlantic (blue line and square symbols; PS2498-1) [*Anderson et al.*, 2014], showing good temporal synchronicity with the dust flux record from EPICA Dome C in Antarctica (black line) [*Lambert et al.*, 2012] over the last ~100 kyr. Note that the EPICA Dome C ice core record is plotted with a logarithmic scaling.

between age tie points at the end and beginning of these intervals, similar to the approach for the preliminary age model of SO202-7-6 presented in section 4.2. For all other core depths in SO202-7-6, calendar ages were assigned by assuming constant sediment accumulation rates between the nearest two age model tie points, either dust tie points or radiocarbon samples (Figure 7).

Linear sedimentation rates (LSRs), resulting from the linear interpolation between age model tie points, range between 2 and 7 cm/kyr in the intervals of 130.5–72.5 cm (27,359–15,197 year B.P.) and 30.5–4.5 cm core depth (11,004–3894 year B.P.), and are slightly higher with ~7–20 cm/kyr between 72.5 and 30.5 cm core depth (15,197–11,004 year B.P.) (Figure 7). The time period with larger LSRs mainly covers the B/A, a warm interstadial that is characterized by a significant increase in deposition of biogenic components (biogenic opal, calcium carbonate, and organic carbon) compared to HS1 and the YD [e.g., *Crusius et al.*, 2004; *Jaccard et al.*, 2009; *Brunelle et al.*, 2010; *Kohfeld and Chase*, 2011; *Lam et al.*, 2013]. As we observe only a slight decrease in eolian dust supply during the B/A, we conclude that the higher LSR spanning the B/A is a result of greater biogenic component deposition.

4.6. Global Potential of Eolian Dust Records as a Chronometer

The evidence provided above indicates that eolian dust records can be applied as a chronostratigraphic tool for marine sediment cores from the western SNP, especially for time periods of sudden climatic transitions like the last deglaciation. The application of this tool can be of high significance in other regions of the global ocean.

A potentially important region for its application is the Southern Ocean. *Anderson et al.* [2014] and *Lamy et al.* [2014] previously observed good temporal synchronicity between lithogenic sediment proxy records from the Southern Atlantic and Pacific Oceans and the dust flux record from the European Project for Ice Coring in Antarctica (EPICA) Dome C ice core in Antarctica [*Lambert et al.*, 2012]. Both sediment studies used the lithogenic sediment proxy data to modify initial age estimates by aligning features in the marine dust records to features in the Dome C dust flux record for the last 800 kyr, similar to an earlier approach by *Petit et al.* [1990]. In Figure 8, we present the marine sediment lithogenic flux record, based on ^{230}Th-normalized ^{232}Th fluxes, from a core in the Subantarctic Atlantic [*Anderson et al.*, 2014] that shows a good correspondence with the Dome C dust flux record in the general pattern of dust flux changes during the last ~100 kyr.

A study from the equatorial Pacific showed that low-latitude dust fluxes, based on ^{230}Th-normalized ^{232}Th fluxes, are also well correlated with records of global ice volume and of eolian dust supply to Antarctica over multiple glacial cycles without any age model adjustment using the dust flux records [*Winckler et al.*, 2008]

(Figure 8). Since age control of marine sediments in the equatorial Pacific was determined independently and since the equatorial Pacific and Antarctica are characterized by different dominant dust sources, the good correlation of the two records provides evidence that dust generation in interhemispheric source regions exhibits a coherent temporal response to climate change [*Winckler et al.*, 2008; *McGee et al.*, 2010], following the principle that different components of Earth's climate system are likely to change concurrently during periods of climate change [e.g., *Alley et al.*, 2003].

While several factors, including source strength, wind patterns, and washout, affect dust deposition, published dust data from different regions of the global ocean show good temporal correspondence to climatic and dust flux changes documented in ice cores over different time scales, indicating the potential of using eolian dust records as a chronometer. If a correlation between dust flux and climate can be established for different regions, after careful and rigorous testing, then eolian dust may be reliably employed as a chronostratigraphic tool in regions without physical connection to a specific, or precisely known, dust source.

5. Summary and Conclusions

Comparing a record of $^4He_{terr}$-based dust fluxes from sediment core SO202-7-6 with the high-resolution dust flux record from the NGRIP ice core [*Ruth et al.*, 2007] provides evidence that there is a good coherence in temporal dust deposition changes in Greenland and the western SNP (Figure 3), two regions with the same dominant dust source, while the amplitude of dust flux variability over the past 27,000 years is much smaller in the western SNP near to the East Asian dust sources, compared to Greenland (Figure 4). The much larger amplitude of variability in the Greenland dust flux record indicates that the efficiency of dust transport to Greenland must have changed synchronously with dust supply, possibly due to climate-related displacement of prevailing winds. This information is crucial for modeling approaches to study the potential climatic impact of dust loading in the atmosphere in the past, present, and future, and it can be used to make a step forward in better understanding the importance of changes in the wind fields versus ocean circulation for climatic changes in glacial and interglacial periods [e.g., *Schmittner*, 2005; *Wunsch*, 2006]. Studies of additional sites will be needed to confirm our observation.

The synchronicity of temporal dust flux changes during the last deglaciation in Greenland and the western SNP, especially at sudden transitions from high to low dust periods, enables the application of high-resolution eolian dust records in marine sediment cores as a chronostratigraphic tool in the western SNP (Figure 5). Synchronicity in abrupt dust deposition changes is further shown between the dust records from Antarctica and marine sediment cores from the Southern Ocean and the equatorial Pacific over the last ~100 kyr (Figure 8), illustrating that the dominant processes regulating dust generation experience a coherent response to global climate change. This indicates that eolian dust records may serve as a chronostratigraphic tool in different regions of the global ocean, and if future studies provide further evidence of synchronous variability, a greater confidence will be gained in using dust records more broadly for age control in paleoceanographic research. This is essential in regions where reliable age determination with common dating techniques is complicated by confounding factors. These regions include the SNP, but also the Southern Ocean characterized by sediments below the carbonate compensation depth and therefore by a limited amount of foraminifera to date. For time periods of short-term pronounced climatic events like the last deglaciation, this chronostratigraphic tool can significantly improve age determination in marine sediments.

Combining three dust-based tie points with a high-resolution planktic foraminiferal radiocarbon stratigraphy, surface water paleoreservoir ages during the last deglaciation can be reconstructed independently, and a reliable age model for core SO202-7-6 could be constructed for the last 27,000 years. The reconstructed paleoreservoir ages for the YD-early Holocene transition, as well as the HS1 and HS2 terminations, overlap within their respective uncertainties (745 ± 140, 680 ± 228, and 790 ± 498 years, respectively) and fall in the range of modern surface water reservoir ages in the western SNP (418–967 years) [*Yoneda et al.*, 2000, 2002, 2004, 2007; *Kuzmin et al.*, 2001, 2007], thereby suggesting that reservoir ages remained relatively constant during the last ~23,000 years. This is in contrast to older paleoreservoir ages during the early last deglaciation reported for the western SNP (945–2150 years) [*Sarnthein et al.*, 2013]. Future studies should examine in more detail the paleoceanographic and ventilation history during the early deglaciation in the western SNP to verify the older paleoreservoir ages documented during this time period.

Acknowledgments
All data for this manuscript are available in Table S1 in the supporting information and through PANGAEA (doi.pangaea.de/10.1594/PANGAEA.845999). INOPEX cores have been obtained during the SO202-INOPEX cruise in July–August 2009 supported by the German Federal Ministry of Education and Research. Financial support for analytical work comes from U.S. NSF through grant OCE1060907 to Gisela Winckler and Robert F. Anderson. Further support was provided by the DFG (German National Science Foundation) through the DFG-Leibniz Center for Surface Process and Climate Studies at the University of Potsdam for Sascha Serno's PhD work and through the NOAA Climate and Global Change Postdoctoral Fellowship program to Haojia Ren. We thank Anders Svensson for his help in constructing the NGRIP dust fluxes, and Roseanne Schwartz, Marty Fleisher, Linda Baker, and Ronny Friedrich at LDEO as well as the technical staff at the NOSAMS and ETH Zürich radiocarbon facilities for technical and laboratory support. The paper was improved by constructive comments of three anonymous reviewers. This is LDEO contribution 7898.

References

Ahagon, N., K. Ohkushi, M. Uchida, and T. Mishima (2003), Mid-depth circulation in the northwest Pacific during the last deglaciation: Evidence from foraminiferal radiocarbon ages, *Geophys. Res. Lett.*, *30*(21), 2097, doi:10.1029/2003GL018287.

Alley, R. B., et al. (2003), Abrupt Climate Change, *Science*, *299*(5615), 2005–2010, doi:10.1126/science.1081056.

Andersen, K. K., et al. (2006), The Greenland Ice Core Chronology 2005, 15–42 ka. Part 1: Constructing the time scale, *Quat. Sci. Rev.*, *25*(23–24), 3246–3257, doi:10.1016/j.quascirev.2006.08.002.

Anderson, R. F., M. P. Bacon, and P. G. Brewer (1983), Removal of ^{230}Th and ^{231}Pa from the open ocean, *Earth Planet. Sci. Lett.*, *62*(1), 7–23, doi:10.1016/0012-821X(83)90067-5.

Anderson, R. F., M. Q. Fleisher, and Y. Lao (2006), Glacial-interglacial variability in the delivery of dust to the central equatorial Pacific Ocean, *Earth Planet. Sci. Lett.*, *242*(3–4), 406–414, doi:10.1016/j.epsl.2005.11.061.

Anderson, R. F., S. Barker, M. Fleisher, R. Gersonde, S. L. Goldstein, G. Kuhn, P. G. Mortyn, K. Pahnke, and J. P. Sachs (2014), Biological response to millennial variability of dust supply in the Subantarctic South Atlantic Ocean, *Philos. Trans. R. Soc., A*, *372*(2019), 20130054, doi:10.1098/rsta.2013.0054.

Bacon, M. P. (1984), Glacial to interglacial changes in carbonate and clay sedimentation in the Atlantic Ocean estimated from ^{230}Th measurements, *Chem. Geol.*, *46*(2), 97–111, doi:10.1016/0009-2541(84)90183-9.

Bacon, M. P., and R. F. Anderson (1982), Distribution of thorium isotopes between dissolved and particulate forms in the deep sea, *J. Geophys. Res.*, *87*(C3), 2045–2056, doi:10.1029/JC087iC03p02045.

Bailey, J. C. (1993), Geochemical history of sediments in the northwestern Pacific Ocean, *Geochem. J.*, *27*(2), 71–90, doi:10.2343/geochemj.27.71.

Ballentine, C. J., and P. G. Burnard (2002), Production, release and transport of noble gases in the continental crust, in *Noble Gases in Geochemistry and Cosmochemistry, Reviews in Mineralogy and Geochemistry*, edited by D. Porcelli, C. J. Ballentine, and R. Wieler, pp. 481–538, Mineral. Soc. of Am., Washington, D. C.

Bhattacharya, A. (2012), Application of the Helium isotopic system to accretion of terrestrial and extraterrestrial dust through the Cenozoic, PhD thesis, Harvard Univ., Cambridge, Mass.

Biscaye, P. E., F. E. Grousset, M. Revel, S. Van der Gaast, G. A. Zielinski, A. Vaars, and G. Kukla (1997), Asian provenance of glacial dust (stage 2) in the Greenland Ice Sheet Project 2 Ice Core, Summit, Greenland, *J. Geophys. Res.*, *102*(C12), 26,765–26,781, doi:10.1029/97JC01249.

Bory, A. J. M., P. E. Biscaye, A. Svensson, and F. E. Grousset (2002), Seasonal variability in the origin of recent atmospheric mineral dust at NorthGRIP, Greenland, *Earth Planet. Sci. Lett.*, *196*(3–4), 123–124, doi:10.1016/S0012-821X(01)00609-4.

Bory, A. J. M., P. E. Biscaye, and F. E. Grousset (2003), Two distinct seasonal Asian source regions for mineral dust deposited in Greenland (NorthGRIP), *Geophys. Res. Lett.*, *30*(4), 1167, doi:10.1029/2002GL016446.

Bromwich, D. H., E. R. Toracinta, H. Wei, R. J. Oglesby, J. L. Fastook, and T. J. Hughes (2004), Polar MM5 Simulations of the Winter Climate of the Laurentide Ice Sheet at the LGM, *J. Clim.*, *17*(17), 3415–3433, doi:10.1175/1520-0442(2004)017<3415:PMSOTW.2.0.CO;2.

Brunelle, B. G., D. M. Sigman, S. L. Jaccard, L. D. Keigwin, B. Plessen, G. Schettler, M. S. Cook, and G. H. Haug (2010), Glacial/interglacial changes in nutrient supply and stratification in the western subarctic North Pacific since the penultimate glacial maximum, *Quat. Sci. Rev.*, *29*(19–20), 2579–2590, doi:10.1016/j.quascirev.2010.03.010.

Bush, A. B. G., and S. G. H. Philander (1999), The climate of the Last Glacial Maximum: Results from a coupled atmosphere–ocean general circulation model, *J. Geophys. Res.*, *104*(D20), 24,509–24,525, doi:10.1029/1999JD900447.

Crusius, J., T. F. Pedersen, S. Kienast, L. Keigwin, and L. Labeyrie (2004), Influence of northwest Pacific productivity on North Pacific Intermediate Water oxygen concentrations during the Bølling-Ållerød interval (14.7–12.9 ka), *Geology*, *32*(7), 633–636, doi:10.1130/G20508.1.

Duplessy, J. C., M. Arnold, E. Bard, A. Juillet-Leclerc, N. Kallel, and L. Labeyrie (1989), AMS ^{14}C study of transient events and of the ventilation rate of the Pacific Intermediate Water during the last deglaciation, *Radiocarbon*, *31*(3), 493–502.

Farley, K. A. (1995), Cenozoic variations in the flux of interplanetary dust recorded by ^{3}He in a deep-sea sediment, *Nature*, *376*(6536), 153–156, doi:10.1038/376153a0.

Farley, K. A. (2001), Extraterrestrial helium in seafloor sediments: Identification, characteristics, and accretion rate over geologic time, in *Accretion of Extraterrestrial Matter Throughout Earth's History*, edited by B. Peucker-Ehrenbrink and B. Schmitz, pp. 179–204, Kluwer Acad., New York.

Fischer, H., M. L. Siggaard-Andersen, U. Ruth, R. Röthlisberger, and E. Wolff (2007), Glacial/interglacial changes in mineral dust and sea-salt records in polar ice cores: Sources, transport, and deposition, *Rev. Geophys.*, *45*, RG1002, doi:10.1029/2005RG000192.

Fleisher, M. Q., and R. F. Anderson (2003), Assessing the collection efficiency of Ross Sea sediment traps using ^{230}Th and ^{231} Pa, *Deep Sea Res., Part II*, *50*(3–4), 693–712, doi:10.1016/S0967-0645(02)00591-X.

Francois, R., M. Frank, M. M. R. van der Loeff, and M. P. Bacon (2004), ^{230}Th normalization: An essential tool for interpreting sedimentary fluxes during the late Quaternary, *Paleoceanography*, *19*, PA1018, doi:10.1029/2003PA000939.

Gersonde, R. (2012), The expedition of the research vessel "Sonne" to the subpolar North Pacific and the Bering Sea in 2009 (SO202-INOPEX), *Rep. Polar Mar. Res.*, *643*, 1–323.

Harrison, S. P., K. E. Kohfeld, C. Roelandt, and T. Claquin (2001), The role of dust in climate changes today, at the Last Glacial Maximum and in the future, *Earth Sci. Rev.*, *54*(1–3), 43–80, doi:10.1016/S0012-8252(01)00041-1.

Haug, G. H., M. A. Maslin, M. Sarnthein, R. Stax, and R. Tiedemann (1995), Evolution of northwest Pacific sedimentation patterns since 6 Ma (Site 882), in *Proceedings of the Ocean Drilling Program, Scientific Results*, vol. 145, edited by D. K. Rea et al., pp. 293–314, Ocean Drilling Program, College Station, Tex.

Haug, G. H., et al. (2005), North Pacific seasonality and the glaciation of North America 2.7 million years ago, *Nature*, *433*(7028), 821–825, doi:10.1038/nature03332.

Henderson, G. M., C. Heinze, R. F. Anderson, and A. M. E. Winguth (1999), Global distribution of the ^{230}Th flux to ocean sediments constrained by GCM modelling, *Deep Sea Res., Part I*, *46*(11), 1861–1893, doi:10.1016/S0967-0637(99)00030-8.

Husar, R. B., et al. (2001), Asian dust events of April 1998, *J. Geophys. Res.*, *106*(D16), 18,317–18,330, doi:10.1029/2000JD900788.

Ikehara, K., K. Ohkushi, A. Shibahara, and M. Hoshiba (2006), Change of bottom water conditions at intermediate depths of the Oyashio region, NW Pacific over the past 20,000 yrs, *Global Planet. Change*, *53*(1–2), 78–91, doi:10.1016/j.gloplacha.2006.01.011.

Jaccard, S. L., E. D. Galbraith, D. M. Sigman, G. H. Haug, R. Francois, T. F. Pedersen, P. Dulski, and H. R. Thierstein (2009), Subarctic Pacific evidence for a glacial deepening of the oceanic respired carbon pool, *Earth Planet. Sci. Lett.*, *277*(1–2), 156–165, doi:10.1016/j.epsl.2008.10.017.

Jickells, T. D., et al. (2005), Global iron connections between desert dust, ocean biogeochemistry, and climate, *Science*, *308*(5718), 67–71, doi:10.1126/science.1105959.

Johnsen, S. J., D. Dahl-Jensen, N. Gundestrup, J. P. Steffensen, H. B. Clausen, H. Miller, V. Masson-Delmotte, A. E. Sveinbjörnsdottir, and J. White (2001), Oxygen isotope and palaeotemperature records from six Greenland ice-core stations: Camp Century, Dye-3, GRIP, GISP2, Renland and NorthGRIP, *J. Quat. Sci.*, *16*(4), 299–307, doi:10.1002/jqs.622.

Jones, C. E., A. N. Halliday, D. K. Rea, and R. M. Owen (1994), Neodymium isotopic variations in North Pacific modern silicate sediment and the insignificance of detrital REE contributions to seawater, *Earth Planet. Sci. Lett.*, *127*(1–4), 55–66, doi:10.1016/0012-821X(94)90197-X.

Jones, C. E., A. N. Halliday, D. K. Rea, and R. M. Owen (2000), Eolian inputs of lead to the North Pacific, *Geochim. Cosmochim. Acta*, *64*(8), 1405–1416, doi:10.1016/S0016-7037(99)00439-1.

Kaufman, Y. J., D. Tanré, and O. Boucher (2002), A satellite view of aerosols in the climate system, *Nature*, *419*(6903), 215–223, doi:10.1038/nature01091.

Keigwin, L. D. (1998), Glacial-age hydrography of the far northwest Pacific Ocean, *Paleoceanography*, *13*(4), 323–339, doi:10.1029/98PA00874.

Keigwin, L. D., G. A. Jones, and P. N. Froelich (1992), A 15,000 year paleoenvironmental record from Meiji Seamount, far northwestern Pacific, *Earth Planet. Sci. Lett.*, *111*(2–4), 425–440, doi:10.1016/0012-821X(92)90194-Z.

Kohfeld, K. E., and Z. Chase (2011), Controls on deglacial changes in biogenic fluxes in the North Pacific Ocean, *Quat. Sci. Rev.*, *30*(23), 3350–3363, doi:10.1016/j.quascirev.2011.08.007.

Kuehn, H., L. Lembke-Jene, R. Gersonde, O. Esper, F. Lamy, H. Arz, and R. Tiedemann (2014), Laminated sediments in the Bering Sea reveal atmospheric teleconnections to Greenland climate on millennial to decadal timescales during the last deglaciation, *Clim. Past*, *10*, 2215–2236, doi:10.5194/cpd-10-2215-2014.

Kuroyanagi, A., H. Kawahata, H. Nishi, and M. C. Honda (2002), Seasonal changes in planktonic foraminifera in the northwestern North Pacific Ocean: Sediment trap experiments from subarctic and subtropical gyres, *Deep Sea Res., Part II*, *49*(24–25), 5627–5645, doi:10.1016/S0967-0645(02)00202-3.

Kurz, M. D., J. Curtice, D. E. Lott, and A. Solow (2004), Rapid helium isotopic variability in Mauna Kea shield lavas from the Hawaiian Scientific Drilling Project, *Geochem. Geophys. Geosyst.*, *5*, Q04G14, doi:10.1029/2002GC000439.

Kutzbach, J. E., and H. E. Wright (1985), Simulation of the climate of 18,000 years BP: Results for the North American/North Atlantic/European sector and comparison with the geologic record of North America, *Quat. Sci. Rev.*, *4*(3), 147–187, doi:10.1016/0277-3791(85)90024-1.

Kuzmin, Y. V., G. S. Burr, and A. J. T. Jull (2001), Radiocarbon reservoir correction ages in the Peter the Great Gulf, Sea of Japan, and eastern coast of the Kunashir, Southern Kuriles (North-western Pacific), *Radiocarbon*, *43*(2A), 477–481.

Kuzmin, Y. V., G. S. Burr, S. V. Gorbunov, V. A. Rakov, and N. G. Razjigaeva (2007), A tale of two seas: Reservoir age correction values (R, ΔR) for the Sakhalin Island (Sea of Japan and Okhotsk Sea), *Nucl. Instrum. Methods Phys. Res., Sect. B*, *259*(1), 460–462, doi:10.1016/j.nimb.2007.01.308.

Lam, P. J., L. F. Robinson, J. Blusztajn, C. Li, M. S. Cook, J. F. McManus, and L. D. Keigwin (2013), Transient stratification as the cause of the North Pacific productivity spike during deglaciation, *Nat. Geosci.*, *6*(8), 622–626, doi:10.1038/ngeo1873.

Lambert, F., M. Bigler, J. P. Steffensen, M. Hutterli, and H. Fischer (2012), Centennial mineral dust variability in high-resolution ice core data from Dome C, Antarctica, *Clim. Past*, *8*(2), 609–623, doi:10.5194/cp-8-609-2012.

Lamy, F., R. Gersonde, G. Winckler, O. Esper, A. Jaeschke, G. Kuhn, J. Ullermann, A. Martinez-Garcia, F. Lambert, and R. Kilian (2014), Increased dust deposition in the Pacific Southern Ocean during glacial periods, *Science*, *343*(6169), 403–407, doi:10.1126/science.1245424.

Levin, Z., E. Ganor, and V. Gladstein (1996), The effects of desert particles coated with sulfate on rain formation in the Eastern Mediterranean, *J. Appl. Meteorol.*, *35*(9), 1511–1523, doi:10.1175/1520-0450(1996)035<1511:TEODPC>2.0.CO;2.

Mahowald, N. M., A. R. Baker, G. Bergametti, N. Brooks, R. A. Duce, T. D. Jickells, N. Kubilay, J. M. Prospero, and I. Tegen (2005), Atmospheric global dust cycle and iron inputs to the ocean, *Global Biogeochem. Cycles*, *19*, GB4025, doi:10.1029/2004GB002402.

Mamyrin, B. A., and I. N. Tolstikhin (1984), *Helium Isotopes in Nature*, Elsevier, Amsterdam.

Manabe, S., and A. J. Broccoli (1985), The influence of continental ice sheets on the climate of an ice age, *J. Geophys. Res.*, *90*(D1), 2167–2190, doi:10.1029/JD090iD01p02167.

Marcantonio, F., D. J. Thomas, S. Woodard, D. McGee, and G. Winckler (2009), Extraterrestrial ^{3}He in Paleocene sediments from Shatsky Rise: Constraints on sedimentation rate variability, *Earth Planet. Sci. Lett.*, *287*(1–2), 24–30, doi:10.1016/j.epsl.2009.07.029.

Martel, D. J., R. K. O'Nions, D. R. Hilton, and E. R. Oxburgh (1990), The role of element distribution in production and release of radiogenic helium: The Carnmenellis Granite, southwest England, *Chem. Geol.*, *88*(3–4), 207–221, doi:10.1016/0009-2541(90)90090-T.

Martin, J. H. (1990), Glacial-interglacial CO_2 change: The Iron Hypothesis, *Paleoceanography*, *5*(1), 1–13, doi:10.1029/PA005i001p00001.

Martinson, D. G., N. G. Pisias, J. D. Hays, J. Imbrie, T. C. Moore, and N. J. Shackleton (1987), Age dating and the orbital theory of the Ice Ages: Development of a high-resolution 0 to 300,000-year chronostratigraphy, *Quat. Res.*, *27*(1), 1–29, doi:10.1016/0033-5894(87)90046-9.

Max, L., J. R. Riethdorf, R. Tiedemann, M. Smirnova, L. Lembke-Jene, K. Fahl, D. Nürnberg, A. Matul, and G. Mollenhauer (2012), Sea surface temperature variability and sea-ice extent in the subarctic Northwest Pacific during the past 15000 years, *Paleoceanography*, *27*, PA3213, doi:10.1029/2012PA002292.

Mayewski, P. A., L. D. Meeker, M. S. Twickler, S. Whitlow, Q. Z. Yang, W. B. Lyons, and M. Prentice (1997), Major features and forcing of high-latitude northern hemisphere atmospheric circulation using a 110,000-year-long glaciochemical series, *J. Geophys. Res.*, *102*(C12), 26,345–26,366, doi:10.1029/96JC03365.

McGee, D. (2009), Reconstructing and interpreting the dust record and probing the plumbing of Mono Lake, PhD thesis, Columbia Univ., New York.

McGee, D., W. S. Broecker, and G. Winckler (2010), Gustiness: The driver of glacial dustiness?, *Quat. Sci. Rev.*, *29*(17–18), 2340–2350, doi:10.1016/j.quascirev.2010.06.009.

McKelvey, B. C., W. Chen, and R. J. Arculus (1995), Provenance of Pliocene-Pleistocene ice-rafted debris, Leg 145, Northern Pacific Ocean, in *Proceedings of the Ocean Drilling Program, Scientific Results*, vol. 145, edited by D. K. Rea et al., pp. 195–204, Ocean Drilling Program, College Station, Tex.

McManus, J. F., R. Francois, J.-M. Gherardi, L. D. Keiwgin, and S. Brown-Leger (2004), Collapse and rapid resumption of Atlantic meridional circulation linked to deglacial climate changes, *Nature*, *428*(6985), 834–837, doi:10.1038/nature02494.

Mukhopadhyay, S., and P. Kreycik (2008), Dust generation and drought patterns in Africa from helium-4 in a modern Cape Verde coral, *Geophys. Res. Lett.*, *35*, L20820, doi:10.1029/2008GL035722.

Mukhopadhyay, S., K. A. Farley, and A. Montanari (2001), A 35 Myr record of helium in pelagic limestones from Italy: Implications for interplanetary dust accretion from the early Maastrichtian to the middle Eocene, *Geochim. Cosmochim. Acta*, *65*(4), 653–669, doi:10.1016/S0016-7037(00)00555-X.

Nagashima, K., R. Tada, A. Tani, Y. Sun, Y. Isozaki, S. Toyoda, and H. Hasegawa (2011), Millennial-scale oscillations of the westerly jet path during the last glacial period, *J. Asian Earth Sci.*, *40*(6), 1214–1220, doi:10.1016/j.jseaes.2010.08.010.

Nier, A. O., and D. J. Schlutter (1990), Helium and neon isotopes in stratospheric particles, *Meteoritics*, *25*(4), 263–267, doi:10.1111/j.1945-5100.1990.tb00710.x.

Nier, A. O., and D. J. Schlutter (1992), Extraction of helium from individual interplanetary dust particles by step-heating, *Meteoritics*, *27*(2), 166–173, doi:10.1111/j.1945-5100.1992.tb00744.x.
Olivarez, A. M., R. M. Owen, and D. K. Rea (1991), Geochemistry of eolian dust in Pacific pelagic sediments: Implications for paleoclimatic interpretations, *Geochim. Cosmochim. Acta*, *55*(8), 2147–2158, doi:10.1016/0016-7037(91)90093-K.
Patterson, D. B., K. A. Farley, and M. D. Norman (1999), ^{4}He as a tracer of continental dust: A 1.9 million year record of aeolian flux to the west equatorial Pacific Ocean, *Geochim. Cosmochim. Acta*, *63*(5), 615–625, doi:10.1016/S0016-7037(99)00077-0.
Petit, J. R., L. Mounier, J. Jouzel, Y. S. Korotkevich, V. I. Kotlyakov, and C. Lorius (1990), Palaeoclimatological and chronological implications of the Vostok core dust record, *Nature*, *343*(6253), 56–58, doi:10.1038/343056a0.
Pettke, T., A. N. Halliday, C. M. Hall, and D. K. Rea (2000), Dust production and deposition in Asia and the North Pacific Ocean over the past 12 Myr, *Earth Planet. Sci. Lett.*, *178*(3–4), 397–413, doi:10.1016/S0012-821X(00)00083-2.
Pisias, N. G., D. G. Martinson, T. C. Moore, N. J. Shackleton, W. Prell, J. Hays, and G. Boden (1984), High resolution stratigraphic correlation of benthic oxygen isotopic records spanning the last 300,000 years, *Mar. Geol.*, *56*(1–4), 119–136, doi:10.1016/0025-3227(84)90009-4.
Porter, S. C., and Z. S. An (1995), Correlation between climate events in the North Atlantic and China during the last glaciation, *Nature*, *375*(6529), 305–308, doi:10.1038/375305a0.
Praetorius, S. K., and A. C. Mix (2014), Synchronization of North Pacific and Greenland climates preceded abrupt deglacial warming, *Science*, *345*(6195), 444–448, doi:10.1126/science.1252000.
Prospero, J. M., P. Ginoux, O. Torres, S. E. Nicholson, and T. E. Gill (2002), Environmental characterization of global sources of atmospheric soil dust identified with the nimbus 7 total ozone mapping spectrometer (TOMS) absorbing aerosol product, *Rev. Geophys.*, *40*(1), 1002, doi:10.1029/2000RG000095.
Ramsey, C. B., et al. (2012), A complete terrestrial radiocarbon record for 11.2 to 52.8 kyr B.P, *Science*, *338*(6105), 370–374, doi:10.1126/science.1226660.
Rasmussen, S. O., et al. (2006), A new Greenland ice core chronology for the last glacial termination, *J. Geophys. Res.*, *111*, D06102, doi:10.1029/2005JD006079.
Rea, D. K., and S. A. Hovan (1995), Grain size distribution and depositional processes of the mineral component of abyssal sediments: Lessons from the North Pacific, *Paleoceanography*, *10*(2), 251–258, doi:10.1029/94PA03355.
Reimer, P. J., et al. (2013), IntCal13 and Marine13 Radiocarbon Age Calibration Curves 0–50,000 Years cal BP, *Radiocarbon*, *55*(4), 1869–1887.
Roe, G. (2009), On the interpretation of Chinese loess as a paleoclimate indicator, *Quat. Res.*, *71*(2), 150–161, doi:10.1016/j.yqres.2008.09.004.
Ruth, U., D. Wagenbach, J. P. Steffensen, and M. Bigler (2003), Continuous record of microparticle concentration and size distribution in the central Greenland NGRIP ice core during the last glacial period, *J. Geophys. Res.*, *108*(D3), 4098, doi:10.1029/2002JD002376.
Ruth, U., M. Bigler, R. Röthlisberger, M. L. Siggaard-Andersen, S. Kipfstuhl, K. Goto-Azuma, M. E. Hansson, S. J. Johnsen, H. Lu, and J. P. Steffensen (2007), Ice core evidence for a very tight link between North Atlantic and east Asian glacial climate, *Geophys. Res. Lett.*, *34*, L03706, doi:10.1029/2006GL027876.
Sarnthein, M., H. Gebhardt, T. Kiefer, M. Kucera, M. Cook, and H. Erlenkeuser (2004), Mid Holocene origin of the sea-surface salinity low in the Subarctic North Pacific, *Quat. Sci. Rev.*, *23*(20–22), 2089–2099, doi:10.1016/j.quascirev.2004.08.008.
Sarnthein, M., B. Schneider, and P. M. Grootes (2013), Peak glacial ^{14}C ventilation ages suggest major draw-down of carbon into the abyssal ocean, *Clim. Past*, *9*(6), 2595–2614, doi:10.5194/cp-9-2595-2013.
Schlitzer, R. (2014), *Ocean Data View*, Alfred Wegener Institute for Polar and Marine Research, Bremerhaven, Germany.
Schmittner, A. (2005), Decline of the marine ecosystem caused by a reduction in the Atlantic overturning circulation, *Nature*, *434*(7033), 628–633, doi:10.1038/nature03476.
Serno, S., G. Winckler, R. F. Anderson, C. T. Hayes, D. McGee, B. Machalett, H. Ren, S. M. Straub, R. Gersonde, and G. H. Haug (2014), Eolian dust input to the Subarctic North Pacific, *Earth Planet. Sci. Lett.*, *387*, 252–263, doi:10.1016/j.epsl.2013.11.008.
Shigemitsu, M., H. Narita, Y. W. Watanabe, N. Harada, and S. Tsunogai (2007), Ba, Si, U, Al, Sc, La, Th, C and ^{13}C/^{12}C in a sediment core in the western subarctic Pacific as proxies of past biological production, *Mar. Chem.*, *106*(3–4), 442–455, doi:10.1016/j.marchem.200704.004.
Steffensen, J. P., et al. (2008), High-resolution Greenland ice core data show abrupt climate change happens in few years, *Science*, *321*(5889), 680–684, doi:10.1126/science.1157707.
Steiger, R. H., and E. Jäger (1977), Subcommission on geochronology: Convention on the use of decay constants in geochronology and cosmochronology, *Earth Planet. Sci. Lett.*, *36*(3), 359–362, doi:10.1016/0012-821X(77)90060-7.
Stuiver, M. (1980), Workshop on C-14 data reporting, *Radiocarbon*, *22*(3), 964–966.
Stuiver, M., and H. A. Pollach (1977), Reporting of C-14 data, discussion, *Radiocarbon*, *19*(3), 355–363.
Stuiver, M., and P. J. Reimer (1993), Extended C-14 data-base and revised Calib 3.0 C-14 age calibration program, *Radiocarbon*, *35*(1), 215–230.
Sun, J. M., M. Y. Zhang, and T. S. Liu (2001), Spatial and temporal characteristics of dust storms in China and its surrounding regions, 1960–1999: Relations to source area and climate, *J. Geophys. Res.*, *106*(D10), 10,325–10,333, doi:10.1029/2000JD900665.
Sun, Y. B., S. C. Clemens, C. Morrill, X. P. Lin, X. L. Wang, and Z. S. An (2012), Influence of Atlantic meridional overturning circulation on the East Asian winter monsoon, *Nat. Geosci.*, *5*(1), 46–49, doi:10.1038/ngeo1326.
Svensson, A., P. E. Biscaye, and F. E. Grousset (2000), Characterization of late glacial continental dust in the Greenland Ice Core Project ice core, *J. Geophys. Res.*, *105*(D4), 4637–4656, doi:10.1029/1999JD901093.
Svensson, A., et al. (2008), A 60000 year Greenland stratigraphic ice core chronology, *Clim. Past*, *4*(1), 47–57, doi:10.5194/cp-4-47-2008.
Taguchi, K., and H. Narita (1995), ^{230}Th and ^{231} Pa distributions in surface sediments off Enshunada, Japan, in *Biogeochemical Processes and Ocean Flux in the western Pacific*, edited by H. Sakai and Y. Nozaki, pp. 375–382, Terra Scientific Publishing, Tokyo, Japan.
Tegen, I., and I. Fung (1994), Modeling of mineral dust in the atmosphere: Sources, transport, and optical thickness, *J. Geophys. Res.*, *99*(D11), 22,897–22,914, doi:10.1029/94JD01928.
Tegen, I., and D. Rind (2000), Influence of the latitudinal temperature gradient on soil dust concentration and deposition in Greenland, *J. Geophys. Res.*, *105*(D6), 7199–7212, doi:10.1029/1999JD901094.
Telford, R. J., E. Heegaard, and H. J. B. Birks (2004), The intercept is a poor estimate of a calibrated radiocarbon age, *Holocene*, *14*(2), 296–298, doi:10.1191/0959683604hl707fa.
Tsoar, H., and K. Pye (1987), Dust transport and the question of desert loess formation, *Sedimentology*, *34*(1), 139–153, doi:10.1111/j.1365-3091.1987.tb00566.x.
Uno, I., K. Eguchi, K. Yumimoto, Z. Liu, Y. Hara, N. Sugimoto, A. Shimizu, and T. Takemura (2011), Large Asian dust layers continuously reached North America in April 2010, *Atmos. Chem. Phys.*, *11*, 7333–7341, doi:10.5194/acp-11-7333-2011.
Vinther, B. M., et al. (2006), A synchronized dating of three Greenland ice cores throughout the Holocene, *J. Geophys. Res.*, *111*, D13102, doi:10.1029/2005JD006921.

Weber, E. T., R. M. Owen, G. R. Dickens, A. N. Halliday, C. E. Jones, and D. K. Rea (1996), Quantitative resolution of eolian continental crustal material and volcanic detritus in North Pacific surface sediment, *Paleoceanography*, *11*(1), 115–127, doi:10.1029/95PA02720.

Winckler, G., and H. Fischer (2006), 30,000 years of cosmic dust in Antarctic ice, *Science*, *313*(5786), 491, doi:10.1126/science.1127469.

Winckler, G., R. F. Anderson, and P. Schlosser (2005), Equatorial Pacific productivity and dust flux during the mid-Pleistocene climate transition, *Paleoceanography*, *20*, PA4025, doi:10.1029/2005PA001177.

Winckler, G., R. F. Anderson, M. Q. Fleisher, D. McGee, and N. Mahowald (2008), Covariant glacial-interglacial dust fluxes in the equatorial Pacific and Antarctica, *Science*, *320*(5872), 93–96, doi:10.1126/science.1150595.

Wolff, E. W., J. Chappellaz, T. Blunier, S. O. Rasmussen, and A. Svensson (2010), Millennial-scale variability during the last glacial: The ice core record, *Quat. Sci. Rev.*, *29*(21–22), 2828–2838, doi:10.1016/j.quascirev.2009.10.013.

Wunsch, C. (2006), Abrupt climate change: An alternative view, *Quat. Res.*, *65*(2), 191–203, doi:10.1016/j.yqres.2005.10.006.

Yancheva, G., N. R. Nowaczyk, J. Mingram, P. Dulski, G. Schettler, J. F. W. Negendank, J. Q. Liu, D. M. Sigman, L. C. Peterson, and G. H. Haug (2007), Influence of the intertropical convergence zone on the East Asian monsoon, *Nature*, *445*(7123), 74–77, doi:10.1038/nature05431.

Yoneda, M., H. Kitagawa, J. van der Plicht, M. Uchida, A. Tanaka, T. Uehiro, Y. Shibata, M. Morita, and T. Ohno (2000), Pre-bomb marine reservoir ages in the western north Pacific: Preliminary result on Kyoto University collection, *Nucl. Instrum. Methods Phys. Res., Sect. B*, *172*(1–4), 377–381, doi:10.1016/S0168-583X(00)00361-X.

Yoneda, M., A. Tanaka, Y. Shibata, and M. Morita (2002), Radiocarbon marine reservoir effect in human remains from the Kitakogane Site, Hokkaido, Japan, *J. Archaeol. Sci.*, *29*(5), 529–536, doi:10.1006/jasc.2001.0764.

Yoneda, M., Y. Shibata, M. Morita, M. Hirota, R. Suzuki, K. Uzawa, N. Ohshima, and Y. Dodo (2004), Interspecies comparison of marine reservoir ages at the Kitakogane shell midden, Hokkaido, Japan, *Nucl. Instrum. Methods Phys. Res., Sect. B*, *223–224*, 376–381, doi:10.1016/j.nimb.2004.04.073.

Yoneda, M., H. Uno, Y. Shibata, R. Suzuki, Y. Kumamoto, K. Yoshida, T. Sasaki, A. Suzuki, and H. Kawahata (2007), Radiocarbon marine reservoir ages in the western Pacific estimated by pre-bomb molluscan shells, *Nucl. Instrum. Methods Phys. Res., Sect. B*, *259*(1), 432–437, doi:10.1016/j.nimb.2007.01.184.